

Corrosion Inhibition and Adsorption Behavior of Some Cationic Surfactants on Carbon Steel in Hydrochloric Acid Solution

A. S. Fouda¹ · M. A. Migahed² · A. A. Atia³ · I. M. Mousa⁴

Received: 13 June 2016/Revised: 27 July 2016/Accepted: 30 July 2016/Published online: 15 August 2016
© Springer International Publishing Switzerland 2016

Abstract The corrosion protection of Cetylpyridinium bromide (CPB) and Cetyltrimethylammonium bromide (CTAB) as cationic surfactant on the corrosion of C-steel in 1 M hydrochloric acid has been studied by weight loss, Tafel polarization, electrochemical impedance spectroscopy, and electrochemical frequency modulation techniques. The carbon steel samples were also analyzed by scanning electron microscopy. The % protection efficiency increases with increasing concentration of the surfactants and decreases with temperature rise. The % protection efficiency reached to 94 % at a concentration of 150 ppm. The protection of C-steel by these surfactants was attributed to the synergistic effect between bromide anions and positive quaternary ammonium ions. The charge transfer resistance increased and double layer capacitance decreased. Surfactant molecules adsorbed on the surface of steel obeys Langmuir adsorption isotherm.

Keywords Carbon steel · HCl · Cationic surfactants · Corrosion inhibition · EIS · EFM · SEM

1 Introduction

Carbon steel is being used extensively under different conditions in industries. Acids are widely used in various technological processes in industry, e.g., in pickling baths, in the extraction and processing oil and gas and in other chemical and petrochemical industries. Also, in the technical cracking of petroleum, acids appear as a result of hydrolysis of salts and may have destructive effect on the equipment. Corrosion due to acids is vital and costly problem in the petroleum refining units and it represents a significant portion of loss because of inefficient operation, lost production, the cost of corrosion control, and high maintenance. To decrease the corrosion of metal, many techniques have been applied; among them, being used are the organic compounds and more specifically cationic surfactants which are increasingly used as corrosion inhibitors. Surfactants are extremely advantageous reagents and they are found at very low quantity in any medium and provide desirable properties to processes in all industries such as paint, coating, food, and petrochemical industry [1]. Surfactants collect in special request at the interfaces and modify the interfaces and in this way control, decrease, or prevent reaction between a substrate and its surroundings, when present in small amount in solution. Different surfactant groups have been accounted for present corrosion inhibitory potential which relies upon the type of surfactants, inhibitor concentration, kind of substrate [2–20], time of immersion in inhibitor solution [6], the presence of salts [21–34], co-surfactant [35, 36], temperature [37–43], structure of inhibitor [44], and the kind of corrosive [8]. In the previous studies, SDBS [45], dithizone and thiosemicarbazide [46], benzyl triethanol ammonium chloride [47], cetyltrimethylammonium bromide, etc., have been studied as corrosion inhibitors for steel in acidic

✉ A. S. Fouda
asfouda@hotmail.com

¹ Department of Chemistry, Faculty of Science, El-Mansoura University, El-Mansoura 35516, Egypt

² Petroleum Research Institute, Nasr City, Cairo, Egypt

³ Department of Chemistry, Faculty of Science, Benha University, Benha, Egypt

⁴ Agricultural Researches Center, Giza, Egypt

medium. The existing data show that the most organic inhibitors act by adsorption on the metal surface. Surfactant inhibitors have many advantages, for example, high inhibition efficiency, low price, low toxicity, and easy production [48, 49]. In this study, the corrosion inhibition of carbon steel in 1 M HCl solution in the absence and presence of investigated Cetylpyridinium bromide (CPB) and Cetyltrimethylammonium bromide (CTAB) has been studied using chemical and electrochemical techniques. The effects of temperature and dose have been studied. The surface morphology of the carbon steel surface after exposing to corrosive medium and at optimum concentration is also utilized by SEM.

2 Experimental

2.1 Chemicals and Materials

Cetyltrimethylammonium bromide (CTAB) and Cetylpyridinium bromide (CPB) were obtained from Sigma-Aldrich. The structures of these surfactants are shown in Table 1. HCl (37.5 %), C₂H₅OH, and (CH₃)₂CO were bought from El-Gomhouria Company, Egypt. Bidistilled water was utilized for all preparations. Composition of carbon steel (weight%) used is as follows: C 0.200, Mn 0.350, P 0.024, Si 0.003, and the remainder Fe.

2.2 Methods

2.2.1 Mass Reduction Technique

For weight reduction estimations, square coins of steel of size (21 × 22 × 1.5 mm) were utilized. The test coins

were rubbed with various grades of emery papers up to 1200 grit size, degreased with (CH₃)₂CO, then washed several times with bidistilled water, and lastly dried between filter papers. The mass reduction tests were performed in a 150-ml beaker placed in bath of water thermostat. The samples were quickly placed in the test solution with 1 M HCl in the presence and absence of various surfactants. After diverse submersion times (30–180 min), the coins were taken out, washed with bidistilled water, dried, and accurately weighed. Triplicate coins were exposed for every condition and the mean weight loss had been accounted. The mass reduction qualities were utilized to measure the rate of corrosion and the protection efficiency from the following equations:

$$\text{C.R.} = \rho \times W/T \times A \times D, \quad (1)$$

where C.R. is the rate of corrosion, ρ is the constant; W is the mass loss (mg), T is the corrosion period (h), A is the specimen area cm², and D is the density (g/cm³). The protection efficiency ($\% \eta$) and degree of metal surface coverage (θ) were measured using the following Eq. (1):

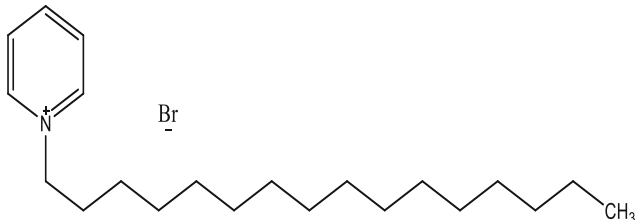
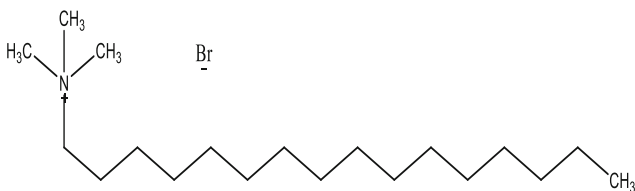
$$\% \eta = 100 \times \theta = [(C.R.* - C.R.) / C.R.*] \times 100, \quad (2)$$

where η is the protection efficiency and C.R.* and C.R. are the rates of corrosion without and with investigated surfactants, respectively.

2.2.2 Electrochemical Methods

Electrochemical techniques were performed in three electrodes thermostatic cell conventional assembly that utilized a Gamry Galvanostat/ZRA/Potentiostat (model PCI 300/4); a sheet of platinum and saturated calomel electrode (SCE) were used as counter and reference electrodes, respectively

Table 1 Molecular structures, molecular weights, and molecular formulae of investigated surfactants

Comp	Structure formulae	Mol. weights	Mol. formulae
CPB		384.44	C ₂₁ H ₃₈ NBr
CTAB		364.45	C ₁₉ H ₄₂ NBr

The working electrode was in the form of a square cut from CS sheet of equal composition embedded in epoxy resin of polytetrafluoroethylene so that the flat surface area was 1 cm². Prior to each measurement, the electrode surface was pretreated in the same manner as the weight loss experiments. Before measurements, the electrode was immersed in solution at natural potential for 30 min until a steady state was reached. The potential was started from -1.2 to +0.2 V versus open circuit potential (E_{ocp}) at a scan rate of 0.5 mVs⁻¹. All experiments were carried out in freshly prepared solutions at 30 °C, and the results were repeated at least three times to check the reproducibility. $\% \eta$ and (θ) were measured from Eq. (3):

$$\% \eta = 100 \times \theta = \left[1 - \left(\frac{i_{corr}^{\circ}}{i_{corr}} \right) \right] \times 100, \tag{3}$$

where i_{corr} and i_{corr}° are the current of corrosion in surfactant solution and in HCl, respectively.

2.2.3 EIS Technique

Impedance measurements were carried out using AC signals of 5 mV peak-to-peak amplitude at the open circuit potential in the frequency range from 10⁵ to 0.1 Hz. The equivalent electrical circuit model utilized for this system is shown in Fig. 1 which consists of a parallel combination of the charge transfer resistance (R_{ct}) and the constant phase element (CPE), both in series with the solution resistance (R_s). CPE is introduced instead of pure double layer capacitance to provide more accurate fit as the double layer at interface does not behave as an ideal capacitor.

Gamry applications used software EIS300 for EIS measurement; computer was utilized for summation of data. Echem Analyst 5.5 software was utilized for fitting, plotting, and graphing data. The protection efficiency ($\% \eta$) and surface coverage (θ) of the surfactant were obtained from the resistance of charge transfer data from the following equation [50]:

$$\% \eta_{EIS} = \theta \times 100 = \left[\frac{(R_{ct} - R_{ct}^*)}{R_{ct}^*} \right] \times 100, \tag{4}$$

where R_{ct}^* and R_{ct} are the charge transfer resistances in the HCl and surfactants, respectively. The interfacial double

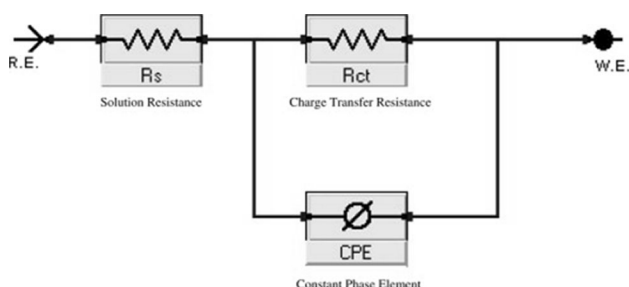


Fig. 1 Electrical equivalent circuit model used to fit the impedance spectra data

layer capacitance (C_{dl}) values were computed from the impedance value [51] by the following equation:

$$C_{dl} = 1/2\pi R_{ct} f_{max}, \tag{5}$$

where f_{max} is the maximum frequency (Hz).

2.2.4 EFM Technique

EFM is a fast and nondestructive experiment technique utilized for the rate of corrosion without prior knowledge of Tafel constants. EFM technique was performed using two frequencies (2.0–5.0 Hz). The choice of the two frequencies was based on three arguments [52]. The larger peaks were used to calculate the corrosion parameters. The steady-state potential was reached after 30 min. The $\% \eta_{EFM}$ was calculated using the Eq. 3.

2.2.5 Surface Analysis

The steel surface was first abraded with different grades of emery papers (grades from 800 to 1200) and washed off using bidistilled water before dipping the specimens for 72 h in 1 M HCl with and without 150 ppm of investigated surfactants. Then, after this immersion time, the specimens were rinsed gently with bidistilled water, carefully dried, and subjected to the surface examination. The surface morphology measurements of the steel surface were carried out using scanning electron microscopy (SEM), the Philips spectrometer (pw-1390) with Cu tube (Cu kal, 1 = 1.54051A°), a scanning electron microscope (SEM, JOEL, JSM-T20, Japan), and energy-dispersive X-ray analysis (EDX) Model HITACHI S-3000H.

2.2.6 Theoretical Study

Quantum chemical measurements were calculated by using Materials Studio software [53]. The following quantum chemical parameters were calculated: dipole moment (μ), highest occupied molecular orbital (HOMO), energy lowest unoccupied molecular orbital (LUMO), energy gap: ΔE ($\Delta E = E_{LUMO} - E_{HOMO}$), and Mulliken charge of the investigated inhibitor.

3 Results and Discussion

3.1 Mass Reduction Tests

The mass reduction–time curves of C-steel with CPB in 1 M HCl at varying doses are shown in Fig. 2. Diagrams for CTAB were given and are shown. This diagram shows that the mass reduction data of C-steel in acid solution in the presence of CPB decreases as its concentration

increases. The variations of the corrosion protection with the surfactant dose are tabulated in Table 2. This trend may result from the fact that the adsorption of inhibitor on the steel increases with the surfactant concentration, and the steel surface is separated from the corrosive medium by the formation of a film on its surface [54]. The lowest protection efficiency ($\% \eta$) is obtained in the presence of CTAB; therefore $\% \eta$ tends to decrease as follows: CPB > CTAB.

3.2 Electrochemical Measurements

3.2.1 Tafel Polarization Tests

The cathodic hydrogen reduction reactions and anodic metal dissolution were hindered and both Tafel slopes are

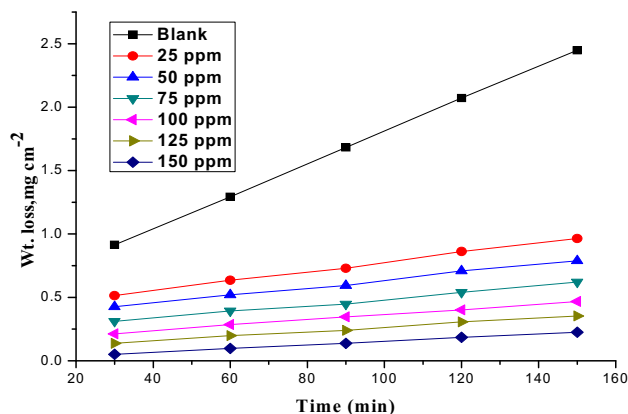


Fig. 2 Weight loss curves for carbon steel dissolution in 1 M HCl in the absence and presence of different doses of CPB at 30 °C

Table 2 Data of weight loss measurements for C-steel in 1 M HCl solution in the absence and presence of different doses of surfactants at 180-min immersion and 30 °C

Comp	Conc. ppm	CR mg cm ⁻² min ⁻¹ × 10 ⁻³	θ	$\% \eta$
Blank	1 M	12.8	–	–
CPB	25	3.76	0.706	70.6
	50	3.05	0.762	76.2
	75	2.55	0.801	80.1
	100	2.08	0.838	83.8
	125	1.79	0.860	86.0
CTAB	150	1.45	0.886	88.6
	25	5.24	0.591	59.1
	50	4.67	0.635	63.5
	75	3.99	0.688	68.8
	100	3.41	0.734	73.4
	125	2.60	0.797	79.7
	150	2.12	0.834	83.4

moved to more positive and more negative potentials compared to the blank plotted (Fig. 3). This behavior is due to the fact that the surfactants act as mixed-type inhibitors [55]. From data obtained, the rise dose of inhibitors leads to a lower in the corrosion current density (i_{corr}), yet the Tafel slopes (β_a, β_c) are consistent showing that the retardation of the two reactions (anodic metal dissolution and cathodic hydrogen reduction) was influenced without changing the dissolution mechanism [18]. The order of protection efficiency was calculated to be CPB > CTAB (Table 3). The $\% \eta$ obtained from potentiodynamic polarization method is close to those obtained from mass reduction calculation. The high $\% \eta$ may due to the adsorption of the surfactants on C-steel surface by horizontal binding to the hydrophobic hydrocarbon chains.

3.2.2 EIS Tests

The EIS was utilized to decide and provide us the kinetic information and important mechanistic for the examined electrochemical system. Nyquist (Fig. 4) and Bode (Fig. 5) impedance curves given from the steel electrode in acid at 25 °C in vicinity and nonappearance of different doses of CPB (the CTAB curves are not appeared). The diagrams show a similar kind of Nyquist drawn for the C-steel with various doses of the surfactants. The presence of single semi-circle leads to the single charge transfer process during dissolution which is unaffected with the presence of surfactant. The difference of the Nyquist curves of the surfactant from perfect semicircles as expected from the theory of EIS is due to dispersion of frequency [56] and impurities, electrode surface heterogeneity resulting from surface roughness, adsorption of inhibitor, dislocations, formation of porous layers, and grain boundaries [57].

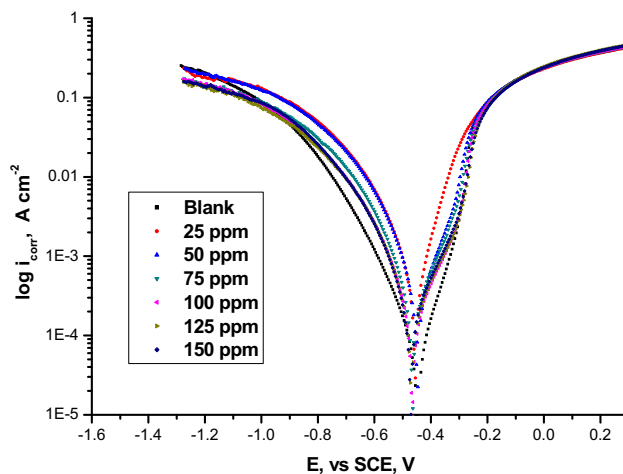


Fig. 3 Potentiodynamic polarization curves for the dissolution of C-steel in 1 M HCl in the absence and presence of different doses of CPB at 30 °C

Table 3 Potentiodynamic data of C-steel in 1 M HCl and in the absence and presence of different doses of surfactants at 30 °C

Comp	Conc, ppm	$-E_{corr}$, versus SCE,V	i_{corr} , mA cm ⁻²	β_c , mV dec ⁻¹	β_a , mV dec ⁻¹	θ	% η
Blank	0.0	0.447	1.73	147	92	–	–
CPB	25	0.532	0.525	167	115	0.697	69.7
	50	0.448	0.426	154	110	0.754	75.4
	75	0.465	0.289	137	116	0.833	83.3
	100	0.465	0.237	181	188	0.863	86.3
	125	0.581	0.167	172	323	0.903	90.3
	150	0.481	0.103	219	151	0.940	94.0
CTAB	25	0.463	0.687	116	123	0.603	60.3
	50	0.462	0.486	113	107	0.719	71.9
	75	0.465	0.382	116	109	0.779	77.9
	100	0.486	0.321	164	121	0.814	81.4
	125	0.479	0.289	130	107	0.833	83.3
	150	0.481	0.203	219	151	0.883	88.3

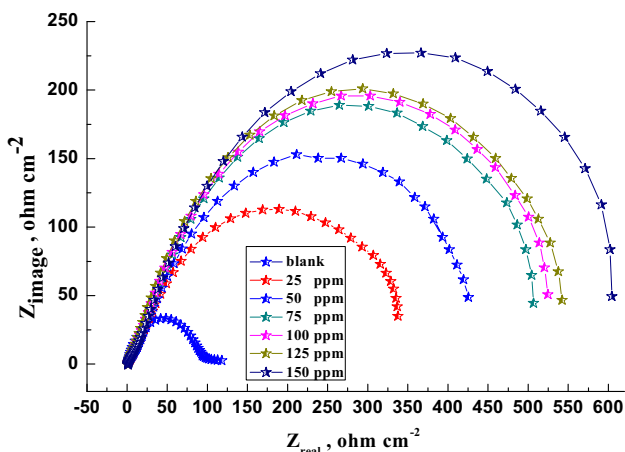


Fig. 4 Nyquist plots for the corrosion of C-steel in 1 M HCl in the absence and presence of different doses of CPB at 30 °C

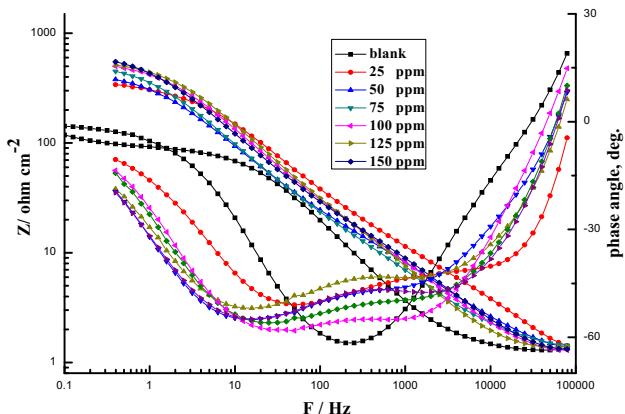


Fig. 5 Bode plots for the corrosion of C-steel in 1 M HCl in the absence and presence of different doses of CPB at 30 °C

Impedance values were calculated by using the circuit as shown in Fig. 1. The information acquired from fitted spectra is shown in Table 4. The information in Table 4 demonstrates that the estimations of R_{ct} increase and the estimations of C_{dl} lowered with the increase in the surfactant doses. Diminish in C_{dl} and increase in R_{ct} data, due to the lower the local dielectric constant (because of the continuous replacement of water molecules by the surfactant molecules on the steel surface) and/or the increase of thickness of the electrical double layer proposed that the inhibitor molecules function by adsorption at the metal/solution surface [58]. The % η given from EIS estimations is in great agreement with that obtained from potentiostatic polarization tests. The difference of inhibition efficiency from the two techniques may be related to various surface status of the electrode in two methods.

Table 4 EIS data of C-steel in the presence and absence of different doses of surfactants at 30 °C

Inhibitor	Conc	C_{dl} μ F cm ⁻²	R_{ct} Ω cm ²	θ	% η
Blank	0.0	1.06	95.53	–	–
CPB	25	2.35	432.9	0.779	77.9
	50	1.63	623.0	0.846	84.6
	75	1.54	661.8	0.855	85.5
	100	1.50	678.2	0.859	85.9
	125	1.37	740.5	0.870	87.0
	150	1.12	906.6	0.894	89.4
CTAB	25	3.48	291.1	0.671	67.1
	50	3.19	318.2	0.699	69.9
	75	3.01	337.1	0.716	71.6
	100	2.06	493.7	0.806	80.6
	125	1.96	519.6	0.816	81.6
	150	1.67	607.1	0.842	84.2

3.3 EFM Tests

EFM is a linear and nondestructive corrosion test technique that can directly determine the corrosion current value without earlier knowledge of Tafel slopes, and with only a small polarizing signal, these advantages of EFM technique make it an ideal technique for online corrosion monitoring [59]. The great strength of the EFM is the causality factors which serve as an internal check on the validity of the EFM tests. Figure 6 shows the EFM spectra for metal with and without various doses of CPB in one molar acid. Spectra for CTAB curves are not appeared). The kinetic parameters such as the causality factors (CF-2 and CF-3), Tafel slopes (β_a and β_c), and the corrosion current density (i_{corr}) are shown in Table 5. The protection efficiency $\% \eta$ increases by expanding the investigated surfactant doses. The causality factors CF-2 and CF-3 are near to their theoretical data showing that the calculated values are of good quality. The measured protection efficiency given from mass reduction, EIS, and potentiostatic polarization methods are of great concurrence with that acquired from EFM technique.

3.3.1 Adsorption Isotherms

Adsorption isotherms were utilized to quantitatively express the adsorption of inhibitors on the metal surfaces. Corrosion protection of metal in acidic media by surfactant is commonly attributed to the adsorption of surfactant on metal surface, and the protection efficiency is directly proportional to the surfactant coverage. The mechanism of the corrosion protection may be explained on the basis of adsorption behavior of the inhibitor. The degree of surface coverage (θ) for different surfactant doses was evaluated from mass loss tests. It is observed that the plot of C/θ versus obeys Langmuir adsorption isotherm through surface coverage of the adsorption of surfactant on C-steel surface. Langmuir isotherm is given by

$$C_{inh}/\theta = 1/K + C_{inh} \tag{6}$$

The plots of C_{inh}/θ versus C_{inh} yielded a straight line with near unit slope for the surfactants (Fig. 7) showing that the adsorption model of the surfactants follows the Langmuir isotherm with good correlation. The higher inhibitive property for the two surfactants is attributed to

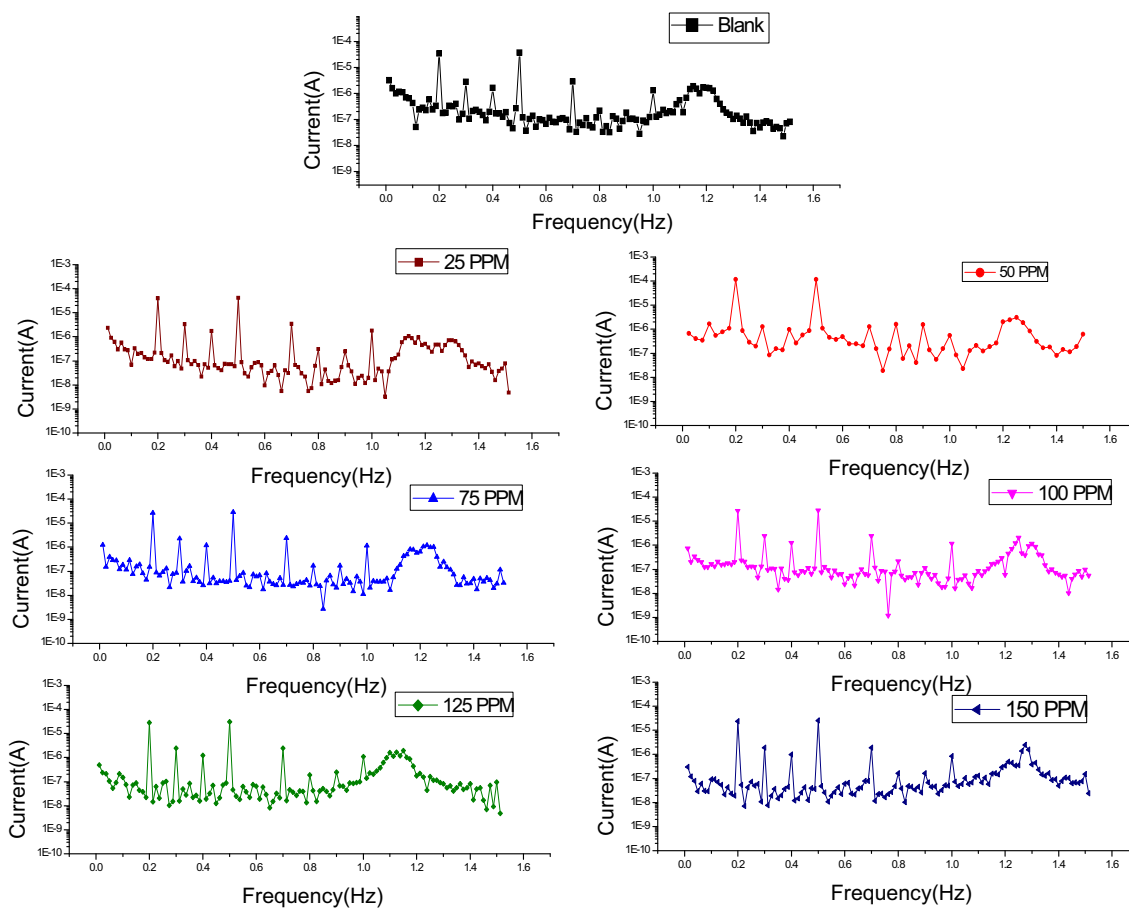


Fig. 6 EFM spectra for carbon steel in the absence and presence of different doses of CPB in 1 M HCl

Table 5 Electrochemical kinetic parameters obtained by EFM technique for C-steel in the absence and presence of various doses of surfactants in 1 M HCl at 30 °C

Inh.	Conc. ppm	i_{corr} $\mu\text{A cm}^{-2}$	β_a mVdec ⁻¹	β_c mVdec-1	CF-2	CF-3	θ	% η
Blank	0.0	258.20	26	32	2.5	3.2	–	–
CPB	25	56.18	99	204	2.5	3.2	0.782	78.2
	50	51.40	76	123	2.0	3.1	0.800	80.0
	75	45.67	114	245	2.1	3.1	0.823	82.3
	100	43.24	125	341	2.0	3.1	0.832	83.2
	125	25.55	114	309	2.1	3.1	0.901	90.1
	150	17.34	121	311	1.9	3.2	0.932	93.2
CTAB	25	82.00	115	120	1.7	3.1	0.682	68.2
	50	80.50	96	104	1.5	3.2	0.688	68.8
	75	75.30	101	103	2.1	3.1	0.708	70.8

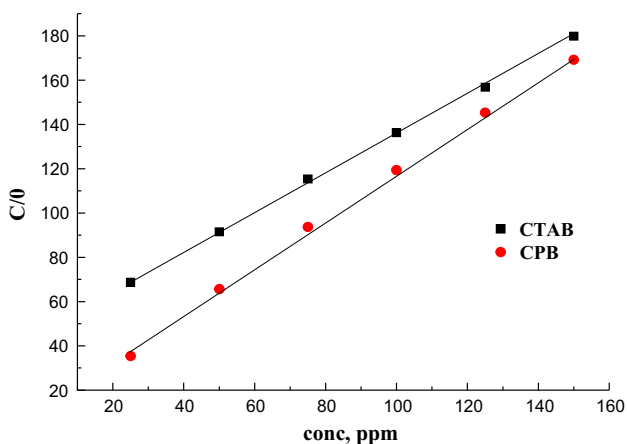


Fig. 7 Langmuir adsorption isotherms for different surfactants from weight loss for C-steel dissolution in 1 M HCl at 30 °C

the presence of quaternary nitrogen atom and the alkyl chain length, which covers greater coverage of the metallic surface [60]. The standard adsorption free energy (ΔG°_{ads}) can be computed using [61]:

$$K_{ads} = 1/55.5 \exp[-\Delta G_{ads}/RT]. \tag{7}$$

The ΔG°_{ads} and K_{ads} values are tabulated in Table 6. These results show that the surfactants are adsorbed on the metal surface physically. The negative ΔG°_{ads} values and

the higher values of K_{ads} lead to the spontaneity of the adsorption process and the stability of adsorbed layer on the steel.

3.3.2 Kinetic Parameters

The temperature effect on the corrosion rate of steel in acid with various doses from surfactant was measured by mass reduction tests over a temperature of 30–50 °C. The effect of increase in temperature on the corrosion rate and % η was calculated using mass loss tests. The results showed that by increasing the temperature, the rate of corrosion increases. Plots of $\log k$ (corrosion rate) versus $1/T$ (temperature absolute) for steel in HCl gave straight lines (Fig. 8). The value of the Arrhenius activation energy (E_a^*) can be obtained using the Arrhenius equation as follows:

$$k = A \exp(-E_a^*/RT), \tag{8}$$

where T represents the absolute temperature, k is the rate of corrosion, A is the Arrhenius constant, and R is the universal gas constant. The (ΔS^\ddagger) entropy and (ΔH^\ddagger) enthalpy of activation can be obtained from the transition state-type equation:

$$k = RT/Nhe^{(\Delta S^\ddagger/R)} e^{(-\Delta H^\ddagger/RT)}. \tag{9}$$

Table 6 Thermodynamic parameters for the adsorption of the investigated CPB in 1 M HCl on the C-steel at different temperatures

	Temp.	Slope	$K_{ads} \times 10^{-3} \text{ M}^{-1}$	R^2	$-\Delta G^\circ_{ads} \text{ kJ mol}^{-1}$
CPB	303	1.0553	1.2695	0.999	9.9
	308	1.0632	1.2332	0.999	9.8
	313	1.1521	0.7127	0.999	9.4
	318	1.1787	0.2768	0.999	8.9
	323	1.3716	0.1501	0.999	8.5
CTAB	303	1.0674	0.0879	0.991	8.2
	308	1.1702	0.0369	0.999	7.8
	313	0.9675	0.0164	0.999	7.2
	318	0.8176	0.0119	0.998	7.0
	323	0.9923	0.0100	0.998	8.7

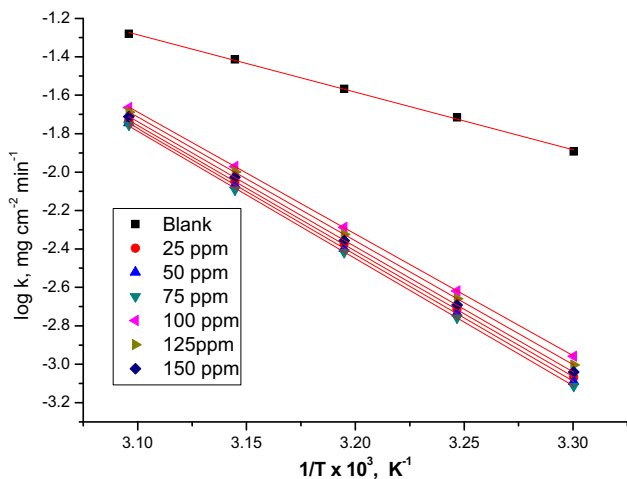


Fig. 8 Arrhenius plots ($\log k$ vs. $1/T$) for corrosion of carbon steel in 1 M HCl in the absence and presence of different doses of CPB

The plots between $\log k/T$ against $1/T$ lead to straight lines; from its slope and intercept, ΔH^* and ΔS^* can be computed, respectively (Fig. 9). Table 7 displays the values of activation parameters for steel dissolution in 1 M HCl solution. It is clear that the value of E_a^* in the presence of CPB and CTAB is higher than that in its absence. These results are in accordance with the studies reported before. The increase of E_a^* in the presence of the surfactants indicates physical adsorption or weak chemical bonding between the surfactant molecules and the C-steel surface. Accordingly, the higher E_a^* values lead to the lower corrosion rate; therefore, the decrease in corrosion rate is mostly decided by the apparent activation energy. This is due to the formation of a film on the carbon steel surface serving as an energy barrier for the carbon steel corrosion; enthalpy and entropy of activation (ΔH^* , ΔS^*) of the corrosion process were measured from the transition state

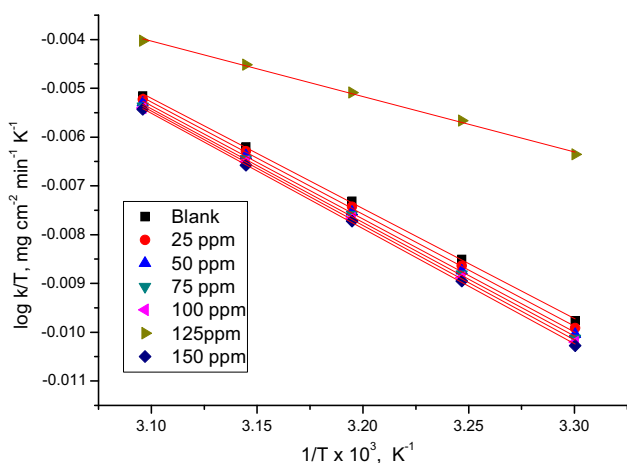


Fig. 9 Plots of ($\log k/T$) versus $1/T$ for corrosion of carbon steel in 1 M HCl in the absence and presence of different doses of CPB

Table 7 Thermodynamic activation parameters of carbon steel dissolution in 1 M HCl in the absence and presence of different doses of surfactants

Inhibitor	Conc., ppm	Activation parameters		
		$-E_a^*$ kJ mol ⁻¹	$-\Delta H^*$ kJ mol ⁻¹	$-\Delta S^*$ J mol ⁻¹ K ⁻¹
Free acid	0.0	62.7	60.1	83.9
CPB	25	85.3	82.7	30.0
	50	90.7	88.1	13.5
	75	93.1	90.5	27.0
	100	95.0	92.4	21.9
	125	96.6	100.0	21.5
	150	97.0	104.4	34.7
CTAB	25	80.1	82.3	26.4
	50	85.9	90.8	22.5
	75	87.6	85.0	22.1
	100	90.5	90.9	34.0
	125	91.2	93.6	32.2
	150	93.9	94.3	36.4

theory [62]. The positive signs of ΔH^* reflect the endothermic nature of the dissolution of metal process. Large and negative ΔS^* imply that the activated complex in the rate-determining step represents an association rather than dissociation step, given that lower disordering takes place from reactants to the activated complex [63].

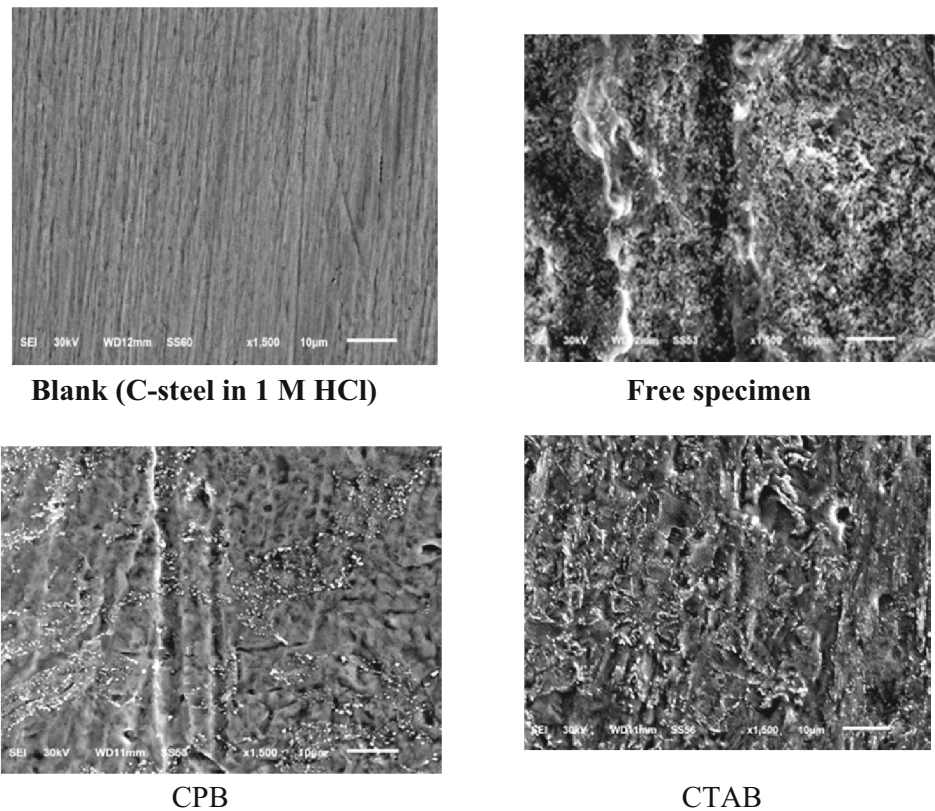
3.3.3 Surface Analysis

The micrographs for C-steel specimen with and without addition of 150 ppm surfactants after 72-h immersion are shown in Fig. 10. This figure shows that in HCl, the steel surface suffers from severe corrosion attack; but in the presence of the surfactants, the steel surface became smoother and the morphology of metal surface is quite different from the previous one. Also, the presence of a film which is distributed in a random way on all surface of steel was noted. Because the adsorption of the surfactants on the metal surface in order to obstruct the active sites which present on surface.

3.3.4 Quantum Parameters of Surfactants

The lower the data obtained from the lowest unoccupied molecular orbital (E_{LUMO}), the higher the capacity of the atom to accept electrons [64]. While the higher data of the highest occupied molecular orbital (E_{HOMO}) of the inhibitor given the easier offering electrons to the empty d-orbital of metal surface lead to the higher in its inhibition efficiency, Fig. 11. Table 8 shows the quantum chemical

Fig. 10 SEM micrographs for carbon steel in the absence and presence of 150 ppm for CPB and CTAB



analyses obtained by VAMP method. The analyses data showed that the CPB has the highest E_{HOMO} , which is expected to have the higher corrosion protection than CTAB. The lower the value of energy gap (ΔE) leads to the increase in the probable protection efficiency of the compound [4]. As shown from Table 8, CPB atom has the smaller energy gap contrast to CTAB. Appropriately, it could be observed that CPB has more inclination to adsorb on the steel surface than CTAB. The higher value of μ leads to the more probable protection efficiency than the other compounds. The calculation shows that the largest data of μ are assigned for CPB, which has the largest protection efficiency, absolute hardness, and softness σ that are the important properties to calculate the molecule stability and reactivity. A hard molecule has a higher energy gap and a soft molecule has a lower energy gap; in a corrosion system, the metal plays as a Lewis acid and the inhibitor plays as a Lewis base, whereas bulk metals are soft acids and thus soft base inhibitors are most effective for acidic corrosion of those metals. It is reported that inhibitor with the largest σ data has the increasing inhibition efficiency (Table 8) which is in great concurrence with the experimental information. The measure listed in Table 8 showed that CPB exhibits some data of global hardness. It means that this one has increased reactivity and the biggest corrosion inhibition than CTAB. This

expectation is in good agreement with the experimental information. The position of the surfactant (lying vertically) could be the purpose behind the increased inhibitor efficiency.

3.3.5 Mechanism of Inhibition

The feasible adsorption of organic cations in the presence of the halide ions is due to the formation of intermediate bridge and the negative ends of the halide metal dipoles being oriented toward the solution, whereby setting up an additional potential difference between the metal and the solution. This will shift the zero charge potential positively. This shift will make the charge on the metal surface more negative and facilitates the adsorption of positively charged surfactant compound by the formation of ionic bonds. High hardness of Br^- ions (counter ion effect) and cationic part of CPB and CTAB suggested higher tendency of an electrostatic adsorption of CPB and CTAB to occur (Cooperative effect) and this leads to a high protection. The adsorption of these two molecules can be described by two main types of interaction: physical and chemical adsorption. Physical adsorption requires the presence of charged metal surface and the charged species in solution, while chemical adsorption involves charge transfer from the species and the metal surface to form coordinate bond.

Fig. 11 The frontier molecular orbital density distribution for CPB and CTAB (HOMO and LUMO)

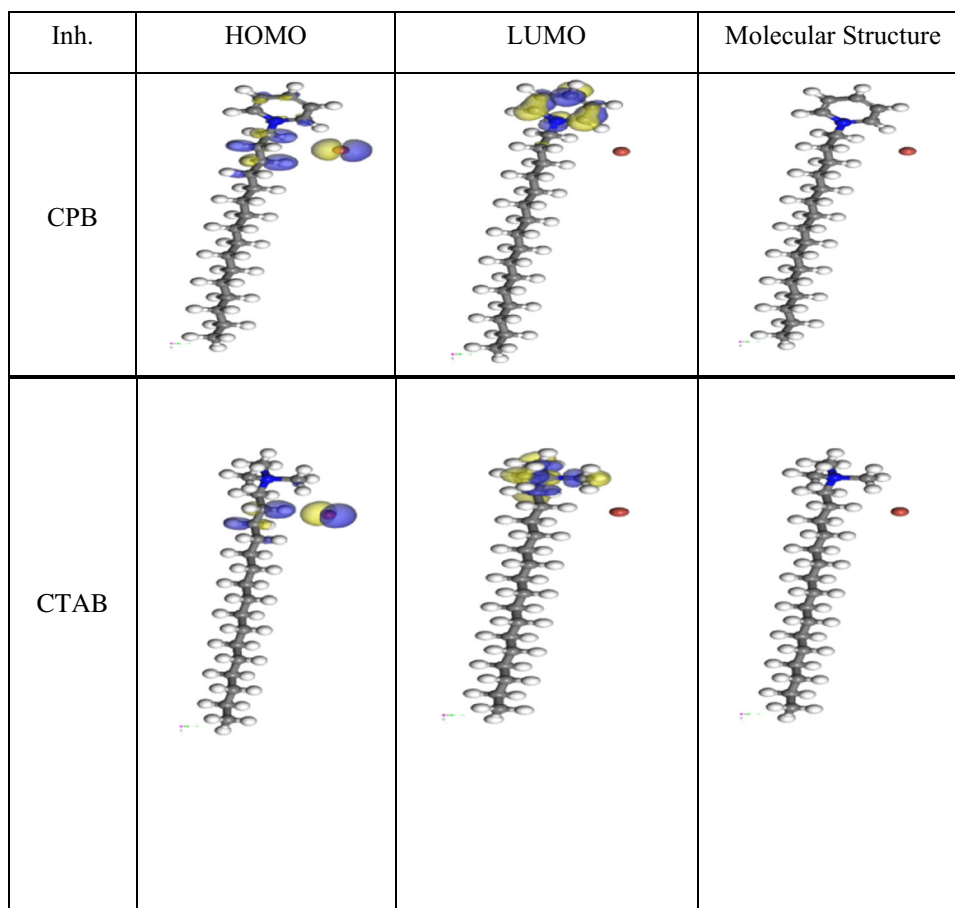


Table 8 Calculated quantum chemical properties for investigated surfactants

Property	E_{HOMO} (eV)	E_{LUMO} (eV)	ΔE	η (eV)	Σ (eV^{-1})	-Pi (eV)	χ (eV)	μ (Debye)
CPB	-10.697	-1.16	9.537	4.769	0.210	5.929	-5.929	21.905
CTAB	-10.845	0.097	10.942	5.471	0.183	5.374	-5.374	20.563

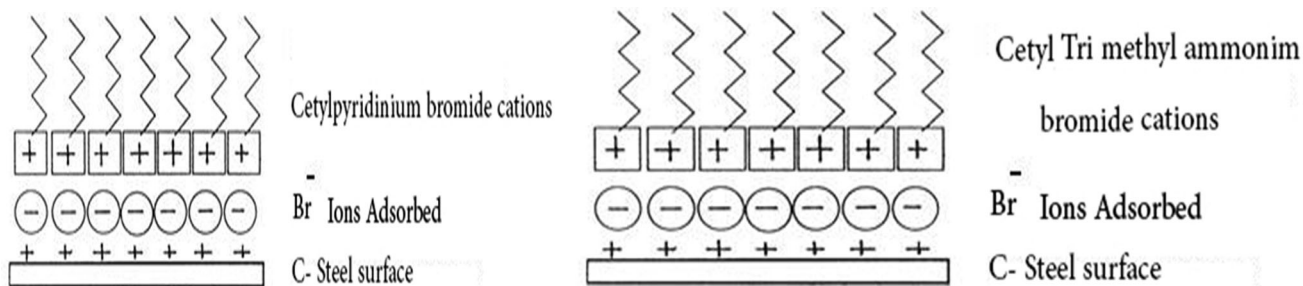


Fig. 12 The expected scheme of adsorption of CPB and CTAB inhibitor on C-steel surface

C-steel surface bears positive charge, Br^- can be adsorbed on C-steel surface making it negatively charged, so the inhibitive action of the two surfactants can result from physical (electrostatic) adsorption of the positive charge of nitrogen to the negatively charged C-steel (Br^- ions act as an adsorption mediator for bonding the two positive

partners, the metal surface and the positively charged surfactant compound). This gives rise to the formation of an adsorption composite film in which the Br^- anions are sandwiched between the metal and positively charged part of the inhibitor [65], see Fig. 12. Besides, the two surfactants may chemisorbed at metal/solution interface by a

coordinate bond which may be formed between the lone electrons pairs of nitrogen atom and the vacant d-orbital of iron atom. Also, pyridinium ring in case of CPB has more π -electrons owing to aromatic ring; it can be also adsorbed on C-steel surface on the basis of donor–acceptor interactions between π -electrons of the pyridinium ring and vacant d-orbital of iron atoms. Inhibition efficiency of CPB is higher than CTAB, this may be due to the fact that the two surfactants are changed in ionic quality, and hence it is found that CPB has ionic quality higher than CTAB in acidic arrangement and lower CMC [66]. Also, CPB has a higher molecular size and one heteroatom than CTAB.

4 Conclusions

CPB and CTAB act as good corrosion inhibitors for C-steel in 1 M HCl medium. The η increases with increasing doses and decreases with increasing the temperature. The inhibition mechanism is explained by adsorption. The adsorption of CPB and CTAB obeys Langmuir adsorption isotherm. CPB and CTAB act as mixed-type inhibitors for C-steel in 1 M HCl medium. The thermodynamic parameters calculated from adsorption isotherm showed that physisorption is involved in the inhibition process. The theoretical information of molecules is in great concurrence with the experimental information. Results obtained from different techniques are in reasonably good agreement.

References

- Agustyn M (2004) European coatings conference, p 19
- Bjelopavlic M, Ralston J, Reynolds G (1998) Adsorption of monoalkyl phosphates at the zircon–aqueous solution interface. *J Colloid Int Sci* 208:183–190
- Deyab MA (2007) Effect of cationic surfactant and inorganic anions on the electrochemical behavior of carbon steel in formation water. *Corros Sci* 49:2315–2328
- Li X, Deng S, Mu G, Fu H, Yang F (2008) Inhibition effect of nonionic surfactant on the corrosion of cold rolled steel in hydrochloric acid. *Corros Sci* 50:420–430
- Abd El Rehim SS, Hassan HH, Amin MA (2004) Inhibition effect of nonionic surfactant on the corrosion of cold rolled steel in hydrochloric acid. *Corros Sci* 46:5–25
- Ma H, Chen S, Yin B, Zhao S, Liu X (2003) Impedance spectroscopic study of corrosion inhibition of copper by surfactants in the acidic solutions. *Corros Sci* 45:867–882
- Free ML (2002) Development and Application of useful equations to predict corrosion inhibition by different surfactants in various aqueous environments. *Corrosion* 58(12):1025–1030
- Soror TY, El-Ziady MA (2002) Effect of cetyltrimethyl ammonium bromide on the corrosion of carbon steel in acids. *Mater Chem Phys* 77:697–703
- Rudresh HB, Mayanna SM (1979) The synergistic effect of Halide ions on the corrosion inhibition of zinc by *n*-decylamine. *Corros Sci* 19:361–370
- Li X, Deng S, Fu H, Mu G (2009) Synergistic inhibition effect of rare earth cerium(IV) ion and 3,4-dihydroxybenzaldehyde on the corrosion of cold rolled steel in H_2SO_4 solution. *Corros Sci* 51:2639–2651
- Murakawa T, Kato T, Nagaura Sh, Hackerman N (1968) A contribution to the understanding of the synergistic effect of anions for the corrosion inhibition of Fe by amines. *Corros Sci* 8:483–489
- Obot IB, Obi-Egbedi NO, Umoren SA (2009) The synergistic inhibitive effect and some quantum chemical parameters of 2, 3-diaminonaphthalene and iodide ions on the hydrochloric acid corrosion of aluminium. *Corros Sci* 51:276–282
- Okafor PC, Zheng Y (2009) Synergistic inhibition behaviour of methylbenzyl quaternary imidazole derivative and iodide ions on mild steel in H_2SO_4 solutions. *Corros Sci* 51:850–859
- Murakawa T, Nagaura S, Hackerman N (1967) Coverage of iron surface by organic compounds and anions in acid solutions. *Corros Sci* 7:79–89
- Karlsson PM, Baeza A, Palmqvist AEC, Holmberg K (2008) Surfactant inhibition of aluminium pigments for waterborne printing inks. *Corros Sci* 50:2282–2287
- Gopi D, Govindaraju KM, Prakash VCA, Sakila DMA, Kavitha L (2009) A study on new benzotriazole derivatives as inhibitors on copper corrosion in ground water. *Corros Sci* 51:2259–2265
- Free ML (2004) A new corrosion inhibition model for surfactants that more closely accounts for actual adsorption than traditional models that assume physical coverage is proportional to inhibition. *Corros Sci* 46:3101–3113
- Migahed MA, Azzam EMS, Morsy SMI (2009) Electrochemical behavior of carbon steel in acid chloride solution in the presence of dodecyl cysteine hydrochloride self-assembled on, gold nanoparticles. *Corros Sci* 51:1636–1644
- Alsabagh AM, Migahed MA, Awad Hayam S (2006) Reactivity of polyester aliphatic amine surfactants as corrosion inhibitors for carbon steel in formation water (deep well water). *Corros Sci* 48:813–823
- Wang WL, Free ML (2004) Reactivity of polyester aliphatic amine surfactants as corrosion inhibitors for carbon steel in formation water (deep well water). *Corros Sci* 46:2601–2611
- Mu G, Li X, Liu G (2005) Synergistic inhibition between tween 60 and NaCl on the corrosion of cold rolled steel in 0.5 M sulfuric acid. *Corros Sci* 47:1932–1952
- Li X, Tang L, Li L, Mu G, Liu G (2006) Synergistic inhibition between *o*-phenanthroline and chloride ion for steel corrosion in sulphuric acid. *Corros Sci* 48:308–321
- Bilgic S, Yilmaz H (2003) Effect of alkaline metal halides on the corrosion inhibition of steel in sulfuric acid containing benzoic acid. *Mater Chem Phys* 79:5–8
- Jeyaprabha C, Sathiyarayanan S, Venkatachari G (2006) Influence of halide ions on the adsorption of diphenylamine on iron in 0.5 M, H_2SO_4 solutions. *Electrochim Acta* 51:4080–4088
- Umoren SA, Ogbobe O, Igwe IO, Ebenso EE (2008) Inhibition of mild steel corrosion in acidic medium using synthetic and naturally occurring polymers and synergistic halide additives. *Corros Sci* 50:1998–2006
- Çalışkan N, Bilgiç S (2000) Effect of iodide ions on the synergistic inhibition of the corrosion of manganese-14 steel in acidic media. *Appl Surf Sci* 153:128–133
- Bouklah M, Hammouti B, Aouniti A, Benkaddour M, Bouyanzer A (2006) Synergistic effect of iodide ions on the corrosion inhibition of steel in 0.5 M H_2SO_4 by new chalcone derivatives. *Appl Surf Sci* 252:6236–6242
- Umoren SA, Ebenso EE (2007) The synergistic effect of polyacrylamide and iodide ions on the corrosion inhibition of mild steel in H_2SO_4 . *Mater Chem Phys* 106:387–393

29. Asefi D, Arami M, Sarabi AA, Mahmoodi NM (2009) Corrosion inhibition effect of cationic surfactant on steel in acid medium and synergistic effect of chloride ion and some alcohols. *J Color Sci Tech* 4:257–263
30. Sathiyarayanan S, Jeyaprabha C, Venkatachari G (2008) Influence of metal cations on the inhibitive effect of polyaniline for iron in 0.5 M H₂SO₄. *Mater Chem Phys* 107:350–355
31. Sathiyarayanan S, Jeyaprabha C, Muralidharan S, Venkatachari G (2006) Inhibition of iron corrosion in 0.5 M sulphuric acid by metal cations. *Appl Surf Sci* 252:8107–8112
32. Asefi D, Arami M, Sarabi AA, Mahmoodi NM (2009) The chain length influence of cationic surfactant and role of nonionic co-surfactants on controlling the corrosion rate of steel in acidic media. *Corros Sci* 51:1817–1821
33. Anand J, Rao PS, Palaniappan S, Sathyanarayana DN (1998) ZnCl₂-induced changes in the electronic properties of polyaniline—HCl salt and its base. *Synth Met* 95:57–62
34. Dimitriev OP, Kislyuk VV (2002) Interaction of the europium chloride and polyaniline: formation of a novel conductive complex. *Synth Met* 132:87–92
35. Feng Y, Siow KS, Teo WK, Hsieh AK (1999) The synergistic effects of propargyl alcohol and potassium iodide on the inhibition of mild steel in 0.5 M sulfuric acid solution. *Corros Sci* 41:829–852
36. Qiu L-G, Xie A-J, Shen Y-H (2005) Understanding the effect of the spacer length on adsorption of gemini surfactants onto steel surface in acid medium. *Appl Surf Sci* 246:1–5
37. Qiu L-G, Wang Y-M, Jiang X (2008) Synergistic effect between cationic Gemini surfactant and chloride ion for the corrosion inhibition of steel in sulphuric acid. *Corros Sci* 50:576–582
38. Qiu L-G, Xie A-J, Shen Y-H (2004) Understanding the adsorption of cationic Gemini surfactants on steel surface in hydrochloric acid. *Mater Chem Phys* 87:237–240
39. El Achouri M, Infante MR, Izquierdo F, Kertit S, Goultaya HM, Nciri B (2001) Synthesis of some cationic Gemini surfactants and their inhibitive effect on iron corrosion in hydrochloric acid medium. *Corros Sci* 43:19–35
40. Qiu LG, Xie A-J, Shen Y-H (2005) The adsorption and corrosion inhibition of some cationic Gemini surfactants on carbon steel surface in hydrochloric acid. *Corros Sci* 47:273–278
41. Chen Q, Zhang D, Li R, Liu H, Hu Y (2008) Effect of the spacer group on the behavior of the cationic Gemini surfactant monolayer at the air/water interface. *Thin Solid Films* 516:8782–8787
42. Huang W, Zhao J (2006) Adsorption of quaternary ammonium Gemini surfactants on zinc and the inhibitive effect on zinc corrosion in vitriolic solution. *Coll. Surf A* 278:246–251
43. Qiu L-G, Xie A-J, Shen Y-H (2005) A novel triazole-based cationic Gemini Surfactant: synthesis and effect on corrosion inhibition of carbon steel in hydrochloric acid. *Mater Chem Phys* 91:269–273
44. Menger FM, Keiper JS (2000) Gemini surfactants. *Chem Int Ed* 39:1906–1920
45. Luo H, Guan YC, Han KN (1998) Inhibition of mild steel corrosion by sodium dodecyl benzene sulfonate and sodium oleate in acidic solutions. *Corrosion* 54(8):619–627
46. Singh A, Chaudhary RS (1996) Dithizone and thiosemicarbazide as inhibitors of corrosion of type 304 stainless steel in 1.0 M sulphuric acid solution. *Br Corros J* 31(4):300–305
47. Osman MM, Omar AM, Al-Sabagh AM (1997) Corrosion inhibition of benzyl triethanol ammonium chloride and its ethoxylate on steel in sulphuric acid solution. *Mater Chem Phys* 50:271–274
48. Kumar A (2008) Corrosion Inhibition of mild steel in hydrochloric acid by sodium lauryl sulfate (SLS). *E J Chem* 5:275–280
49. El-Azhar M, Mernari B, Traisnel M, Bentiss F, Lagrenee M (2001) Corrosion inhibition of mild steel by the new class of inhibitors [2,5-bis(*n*-pyridyl)-1,3,4-thiadiazoles] in acidic media. *Corros Sci* 43:2227–2238
50. Bentiss F, Lagrenee M, Traisnel M, Hornez JC (1999) The corrosion inhibition of mild steel in acidic media by a new triazole derivative. *Corros Sci* 41:789–803
51. Hsu CH, Mansfeld F (2001) Technical note: concerning the conversion of the constant phase element parameter Y₀ into a capacitance. *Corrosion* 57:747–748
52. Khaled K (2009) Evaluation of electrochemical frequency modulation as a new technique for monitoring corrosion and corrosion inhibition of carbon steel in perchloric acid using hydrazine carbodithioic acid derivatives. *J Appl Electrochem* 39:429–438
53. Javaherdashti R (2000) How corrosion affects industry and life. *Anti Corros Meth Mater* 47:30–34
54. Maayta AK, Al-Rawashdeh NAF (2004) Inhibition of acidic corrosion of pure aluminum by some organic compounds. *Corros Sci* 46:1129–1140
55. Fouda AS, Al-Sarawy AA, El-Katori EE (2006) Pyrazolone derivatives as corrosion inhibitors for C-steel in hydrochloric acid solution. *Desalination* 201:1–13
56. El Achouri M, Kertit S, Goultaya HM, Nciri B, Bensouda Y, Perez L, Infante MR, Elkacemi K (2001) Corrosion inhibition of iron in 1 M HCl by some Gemini surfactants in the series of alkanediyl- α , ω -bis-(dimethyl tetradecyl ammonium bromide). *Prog Org Coat* 43:267–273
57. Growcock FB, Jasinski JH (1989) Time-resolved impedance spectroscopy of mild steel in concentrated hydrochloric acid. *J Electrochem Soc* 136:2310–2314
58. Bessone J, Mayer C, Tuttner K, Lorenz WJ (1983) AC-impedance measurements on aluminium barrier type oxide films. *Electrochim Acta* 28:171–175
59. Bosch RW, Hubrecht J, Bogaerts WF, Syrett BC (2001) Electrochemical frequency modulation: a new electrochemical technique for online corrosion monitoring. *Corrosion* 57:60–70
60. Szklarska-Smiaiowska Z (1991) Electrochemical and optical techniques for the study of metallic corrosion. Kluwer Academic, Dordrecht, p 545
61. Christov M, Popova A (2004) Adsorption characteristics of corrosion inhibitors from corrosion rate measurements. *Corros Sci* 46:1613–1620
62. Zhao TP, Mu GN (1999) The adsorption and corrosion inhibition of anion surfactants on aluminium surface in hydrochloric acid. *Corros Sci* 41:1937–1944
63. Tang LB, Mu G, Liu GH (2003) The effect of neutral red on the corrosion inhibition of cold rolled steel in 1.0 M hydrochloric acid. *Corros Sci* 45:2251–2262
64. Khamis E (1990) The effect of temperature on the acidic dissolution of steel in the presence of inhibitors. *Corrosion* 46:476–484
65. Lipkowsky J, Ross PN (1992) Adsorption of molecules at metal electrodes. VCH, New York
66. El-Sherbiny EF (1999) Effect of some ethoxylated fatty acids on the corrosion behavior of mild steel in sulphuric acid solution. *Mater Chem Phys* 60:286–290